

Vision Inference Former: Sustaining Visual Consistency in Multimodal Large Language Models

Xinpeng Dong^{1*} Min Zhang^{2*} Kairong Han¹ Xu Tan³ Fei Wu¹ Kun Kuang^{1†}

¹Zhejiang University, ²East China Normal University, ³Zhejiang University of Science and Technology

dongxinpeng@zju.edu.cn, mzhang@cs.ecnu.edu.cn, zju_handso@163.com, tanxu@zust.edu.cn

wufei@zju.edu.cn, kunkuang@zju.edu.cn

Abstract

In recent years, multimodal large language models (MLLMs) have achieved remarkable progress, primarily attributed to effective paradigms for integrating visual and textual information. The dominant connector-based paradigm projects visual features into textual sequence, enabling unified multimodal alignment and reasoning within a generative architecture. However, our experiments reveal two key limitations: (1) Although visual information serves as the core evidential modality in MLLMs, it is treated on par with textual tokens, diminishing the unique contribution of the visual modality; (2) As generation length increases, particularly within a limited context window, the model’s dependence on visual information progressively weakens, resulting in deteriorated vision-language alignment and reduced consistency between generated content and visual semantics. To address these challenges, we propose the Vision Inference Former (VIF), a lightweight architectural module that establishes a direct bridge between pure visual representations and the model’s output space. Specifically, VIF continuously injects visual semantics throughout the decoding phase of the inference process, ensuring that the model remains firmly grounded in visual content during generation. We conduct experiments on 14 benchmark tasks covering general reasoning, OCR, table understanding, vision-centric evaluation, and hallucination. Experimental results show that VIF consistently improves model performance across diverse architectures while introducing minimal additional overhead. The code for this work is available¹.

1. Introduction

Multimodal large language models (MLLMs) have recently achieved remarkable progress in bridging vision and language understanding. By combining powerful vision en-

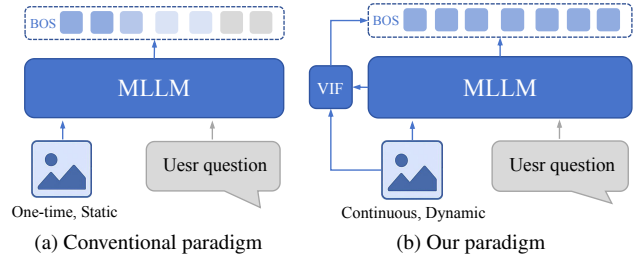


Figure 1. Paradigm comparison. In the conventional paradigm, visual information is statically concatenated with textual sequence and fed into the model once. This static fusion weakens the contribution of visual cues as the primary source of evidence and leads to reduced visual-textual consistency as generation progresses.

coders with large language models (LLMs), MLLMs can perform a wide spectrum of vision-language tasks in a unified generative framework. Recent advances such as GPT-4V [29], Gemini [36], Qwen-VL [6], and LLaVA [20] have demonstrated unprecedented performance on diverse visual question answering (VQA) benchmarks, showing strong visual grounding and reasoning capabilities. These achievements highlight the strong potential of MLLMs to generalize across modalities and to reason over complex visual scenes using natural language, marking a significant milestone toward the goal of unified multimodal intelligence.

Despite these impressive advances, current MLLMs still face a notable limitation in maintaining visual consistency during multimodal reasoning. Although these models exhibit strong answering abilities, they often rely on textual priors, resulting in responses that deviate from the actual image content [16, 35, 47]. A key architectural factor contributing to this issue lies in the common practice of directly concatenating visual tokens with textual sequences. This design treats visual information as an auxiliary prefix rather than a continuously referenced source, causing the model to underutilize fine-grained visual cues during generation. Consequently, as decoding progresses, the influence of visual embeddings tends to diminish, leading to a gradual drift from the input image. We term this phenomenon visual con-

*Equal contribution. †Corresponding author.

¹<https://github.com/Dong-Xinpeng/VIF>



User: Describe this image.



LLaVA: The image captures a busy city street with a man standing on the back of a yellow truck, holding a clothes iron. He appears to be ironing clothes while the truck is in motion. The truck is surrounded by other vehicles, including a taxi and a car, which are driving alongside it. There are several people in the scene, with **one person standing close to the man on the truck and others scattered around the street. A handbag can be seen near the center of the image, possibly belonging to one of the pedestrians.** The overall atmosphere of the scene is bustling and dynamic, showcasing the hustle and bustle of city life.

LLaVA-VIF: The image captures a unique scene on a city street. A man, dressed in a yellow shirt and blue pants, is standing on the back of a yellow SUV. He is holding a blue shirt and appears to be ironing it. The SUV is parked on the side of the street, and there are other cars and buildings in the background. The man's unusual activity and the bright colors of the SUV and the shirt make this image stand out. It's a snapshot of an everyday moment, but with a twist that adds an element of surprise and intrigue.

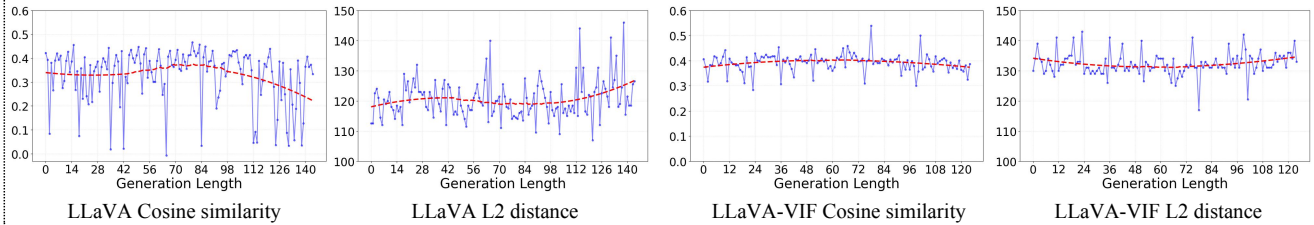


Figure 2. We qualitatively compare LLaVA-1.5 and our LLaVA-1.5-VIF on the same question case. As the generation progresses, LLaVA gradually deviates from the visual content, whereas LLaVA-VIF consistently maintains high fidelity to the image throughout the response. We further illustrate the evolution of image–text correlation with respect to generation length. Specifically, we measure the average cosine similarity and L2 distance between each generated token and all decoded visual tokens. The red line denotes the smoothed trend obtained via a Savitzky–Golay filter [33]. As shown, LLaVA’s cosine similarity decreases and L2 distance increases over time, indicating visual inconsistency, whereas LLaVA-VIF remains stable throughout the generation.

sistency decay. This challenge highlights an urgent need for mechanisms that can reinforce visual grounding throughout the entire generation process.

To address the challenge of visual consistency decay, we introduce the **Visual Inference Former (VIF)**, a lightweight, inference-oriented module aimed to enhance visual consistency during the multimodal reasoning process. As shown in Figure 1, unlike the conventional paradigm of treating image tokens as static context concatenated with the text input, the VIF dynamically interacts with the evolving textual representations throughout the entire decoding sequence. By injecting fine-grained visual information directly into the current hidden state, VIF facilitates the continuous retrieval and integration of pertinent image features, thereby ensuring that visual salience remains influential and consistent throughout the autoregressive generation process.

To further illustrate the efficacy and necessity of VIF, we perform a qualitative comparison between the baseline LLaVA-1.5-7B and our enhanced LLaVA-1.5-7B-VIF model. As depicted in Figure 2, the baseline model increasingly relies on linguistic priors, causing its output to drift away from the visual content as generation progresses, frequently leading to visual-textual misalignment in the latter stages of the output. In contrast, LLaVA-VIF consistently maintains strong visual consistency and generates responses demonstrably faithful to the given image. This qualitative result indicates that the VIF module effectively mitigates

the common problem of visual consistency decay, ensuring the image remains a stable and reliable source of information throughout the entire reasoning process. The module’s efficacy is further substantiated by extensive quantitative experiments across multiple benchmarks, which confirm that our method achieves highly competitive performance on a diverse range of tasks.

We summarize our contributions as follows.

- We systematically identify and analyze the critical issue of visual consistency decay in mainstream MLLMs, which manifests as a gradual neglect of visual information and a consequent deviation from the image content as the output length increases.
- We propose the visual inference former, a lightweight module designed to mitigate visual consistency decay by dynamically injecting fine-grained visual signals into the hidden states at each generation step.
- Comprehensive evaluations on a broad range of benchmarks confirm that integrating VIF brings significant gains, strengthening both multimodal reasoning ability and visual consistency.

2. Related work

2.1. Multimodal large language models

The evolution of multimodal large language models has progressed from task-specific architectures to a universal,

LLM-centric paradigm. Early methods [1, 23] utilized encoder-decoder frameworks with cross-attention, which achieved strong performance on narrow tasks but lacked scalability and transferability due to their reliance on heavy supervision. A pivotal shift occurred with contrastive pre-training frameworks like CLIP [30] and ALIGN [14]. By learning cross-modal correspondences from massive image-text pairs, these models produced robust visual representations aligned with textual semantics. While discriminative in nature, they laid the essential groundwork for today’s generative multimodal reasoning. Building on this foundation, the current LLM-centric paradigm integrates a pretrained vision encoder with an LLM via a lightweight connector. This modular design effectively decouples visual perception (encoder) from high-level reasoning (LLM). Seminal works introduced varied connector strategies: BLIP-2 [17] employed a Q-Former, LLaVA [20] used a simple linear projection, and InstructBLIP [8] introduced a refined MLP-based adapter. Subsequent models, including MiniGPT-4 [48], mPLUG-Owl3 [44], Qwen-VL [42], and InternVL [5], have further advanced this architecture through multi-stage alignment and large-scale instruction tuning, endowing MLLMs with impressive visual question answering abilities.

2.2. Vision language alignment

Effective vision–language alignment serves as the cornerstone of faithful multimodal understanding and generation. Although the “vision encoder + connector + LLM” paradigm has enabled impressive multimodal reasoning, it primarily relies on shallow alignment between visual embeddings and language token spaces. This often results in a model that leverages image features for coarse semantic grounding, yet progressively shifts its focus toward text-only reasoning during generation, leading to visual forgetting or hallucination phenomena.

To address this limitation, a line of research aims to enhance vision–language alignment between visual and linguistic representations. For instance, InternVL-3 [49] enhances semantic integration by co-training both the vision encoder and LLM parameters, thereby enabling bidirectional adaptation between vision and language modules. MetaMorph [38] proposes Visual-Predictive Instruction Tuning (VPiT), transforming a pre-trained LLM into a unified multimodal model capable of processing both visual and textual inputs. AIMv2 [10] employs a pixel-level reconstruction loss to reinforce perceptual grounding, while Ross [40] incorporates an additional diffusion-based module to capture fine-grained visual information and preserve detailed spatial awareness.

While beneficial, these methods primarily focus on improving the visual embedding quality rather than ensuring sustained visual attention during generation. To miti-

gate this, Qwen-LA [6] employs a reinforcement learning strategy that explicitly inserts image tokens into the output sequence, encouraging the model to revisit visual content throughout the decoding process. Similarly, VISTA [18] introduces an alignment loss during pretraining, constraining the output token embeddings to remain semantically close to image representations. These approaches represent a shift from static feature alignment toward dynamic, generation-aware alignment, which ensures that multimodal large language models maintain consistent grounding in visual information when producing textual outputs.

3. Preliminaries

We consider a standard multimodal large language model π_θ that follows the prevalent vision encoder + connector + LLM paradigm. Given an input image I and a textual instruction T , the vision encoder E_v (e.g., ViT [9]) extracts a sequence of visual tokens:

$$V = E_v(I) = [v_1, v_2, v_3, \dots, v_{N_v}] \in R^{N_v \times d_v}, \quad (1)$$

where N_v denotes the number of visual tokens and d_v denotes vision embedding dimension.

A lightweight connector f , implemented as a linear projector, MLP, Q-Former or related architectures, then maps these embeddings into the language model’s input space:

$$Z^v = f(V) = [z_1^v, z_2^v, z_3^v, \dots, z_{N_v}^v] \in R^{N_v \times d_l}, \quad (2)$$

where d_l is the hidden dimension of the LLM.

The resulting visual embeddings Z^v are concatenated with the text embeddings $Z^t = E_t(T) \in R^{N_t \times d_l}$, where E_t is the text encoder. The combined sequence $Z = [Z^v, Z^t]$ is fed into the pretrained large language model M , which autoregressively generates an output sequence $O = [o_1, o_2, o_3, \dots, o_n]$. At each decoding step l , the model predicts the next-token distribution as:

$$p(o_l | o_{<l}, Z) = \text{softmax}(W_o h_l), \quad (3)$$

where W_o denotes the output projection matrix, h_l is the hidden state output from the LLM at step l . The model is trained under the next-token prediction objective:

$$L_{NTP} = - \sum_{l=1}^n \log p(o_l | o_{<l}, Z), \quad (4)$$

encouraging the model to predict the correct next token conditioned on previous tokens.

4. Methodology

In this section, we present an overview of the proposed vision inference former. VIF is a lightweight auxiliary module designed to alleviate the issue of visual consistency

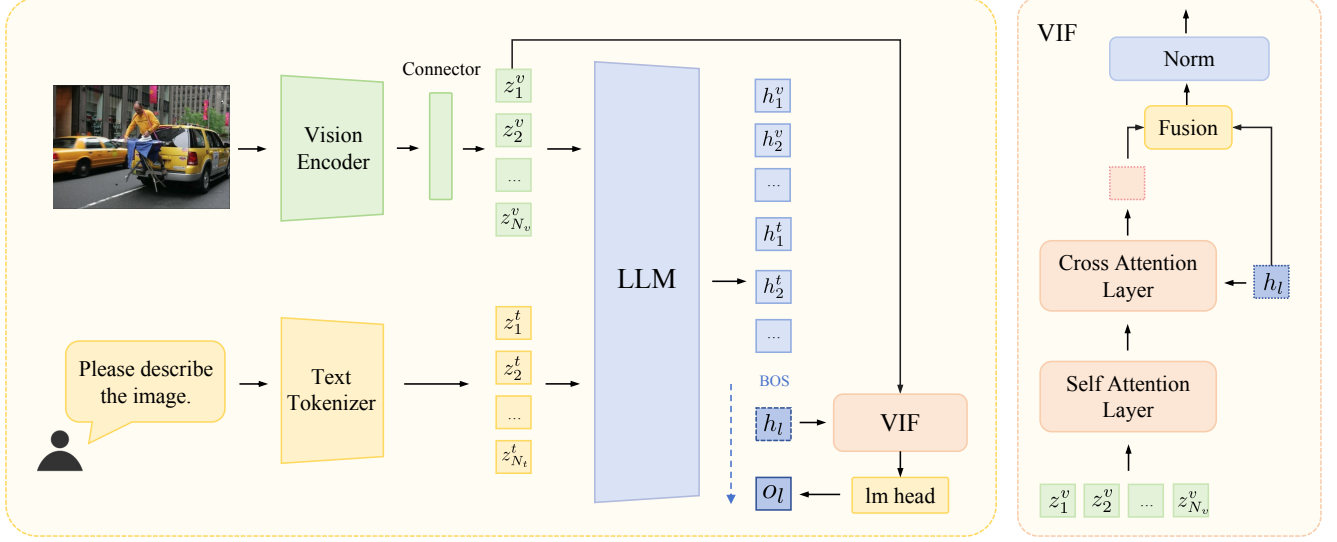


Figure 3. Overall framework. The left figure illustrates the workflow of the VIF module during model inference. The module takes pure visual information and the model’s native hidden states as inputs, injecting visual features into the model’s output representation space to achieve cross-modal fusion. The right figure presents the architecture of our proposed lightweight VIF, which consists of one self-attention layer, one cross-attention layer, and a fusion module.

decay often observed in multimodal large language models. Conceptually, VIF introduces a direct and dynamic interaction pathway between the visual representation space and the model’s final output embedding space. This architecture enables the continuous reinforcement of visual cues throughout the decoding process, independent of the model’s context window size, thereby ensuring stable and fine-grained visual grounding during generation.

4.1. Architecture

As illustrated in Figure 3, the proposed VIF is implemented as a two-layer Transformer module positioned between the visual embeddings Z^v and the LLM hidden states h_l . It comprises two Transformer sub-layers that collaboratively refine visual semantics and adaptively retrieve visual information conditioned on the evolving textual context.

The first Transformer sub-layer performs intra-visual self-attention over the visual embeddings Z^v :

$$\hat{Z}^v = \text{softmax}\left(\frac{Q^v K^{v\top}}{\sqrt{d}}\right)V^v, \quad (5)$$

where Q^v , K^v , and V^v denote the linear projections of Z^v , and d represents the dimensionality of the key vectors. This operation enables each visual token to aggregate local semantic relationships and contextual cues within the image, resulting in refined visual embeddings \hat{Z}^v that better capture intra-image dependencies.

The second Transformer sub-layer performs cross-attention between the refined visual embeddings and the

current hidden state of the LLM h_l :

$$Z^h = \text{softmax}\left(\frac{Q^h \hat{K}^{v\top}}{\sqrt{d}}\right)\hat{V}^v, \quad (6)$$

where the query Q^h is projected from the current textual hidden state, while \hat{K}^v and \hat{V}^v are obtained from the updated visual embeddings \hat{Z}^v . Through this mechanism, the model selectively retrieves contextually relevant visual evidence conditioned on the evolving linguistic context, thereby maintaining coherent and fine-grained visual grounding throughout the generation process.

4.2. Visual textual fusion

The output of VIF Z^h , is fused with the original hidden state of the LLM, h_l , to produce a visually enhanced representation. In this work, we adopt a simple yet effective additive fusion strategy:

$$h'_l = \text{Norm}(Z^h + h_l) \quad (7)$$

where $\text{Norm}(\cdot)$ denotes layer normalization applied after fusion. The resulting fused representation h'_l is subsequently used for next-token prediction:

$$p(o_l | o_{<l}, Z^v, Z^t, A_l) = \text{softmax}(W_o h'_l), \quad (8)$$

where A_l represents the dynamic visual inference state generated by VIF. This fusion is performed at every decoding step, ensuring that image-grounded inference and visual consistency are continuously maintained throughout the entire generation process.

Table 1. Performance comparison on general benchmarks. We highlight the best results in **bold**.

Method	Params	MMBench	MMMU	MMStar	OKVQA	GQA	ScienceQA	Average
GPT-4V-1106	-	75.8	53.8	-	-	-	77.54	-
Gemini Pro	-	73.6	48.9	59.1	-	-	-	-
Cambrian-1	8B	75.9	42.7	-	-	-	64.6	-
mPLUG-Owl3	8B	73.6	48.9	59.1	-	-	-	-
Ross	7B	67.7	36.9	-	-	63.7	-	-
<i>Base model: Qwen-2.5-VL</i>								
Qwen2.5-VL	7B	86.74	50.22	62.06	53.11	79.80	83.69	69.27
Qwen2.5-VL-SFT	7B	86.95	49.67	62.53	56.70	81.37	88.32	70.92
Qwen2.5-VL-VIF	7B	88.54	50.99	65.20	57.79	82.60	93.37	73.08
<i>Base model: LLaVA-1.5</i>								
VISTA	7B	66.08	35.88	35.91	56.30	62.90	-	-
LLaVA-1.5	7B	72.94	35.33	33.00	51.38	76.80	64.04	55.58
LLaVA-1.5-SFT	7B	74.94	36.44	35.53	55.29	80.06	79.35	60.27
LLaVA-1.5-VIF	7B	77.04	37.56	37.07	57.25	81.41	81.16	61.91
LLaVA-1.5	13B	76.67	35.22	33.87	53.69	78.98	65.52	57.33
LLaVA-1.5-SFT	13B	77.85	35.22	39.93	57.37	81.62	82.26	62.37
LLaVA-1.5-VIF	13B	79.16	36.11	41.07	57.06	82.36	85.12	63.48

4.3. Training objective

The proposed VIF module introduces no additional supervision and is jointly optimized with the base MLLM under the standard next-token prediction objective:

$$L_{VIF} = - \sum_{l=1}^N \log p(o_l | o_{<l}, Z^v, Z^t, A_l), \quad (9)$$

This formulation ensures that the model learns to integrate visual and textual information seamlessly within the standard autoregressive training paradigm.

4.4. Analysis

To better understand the effectiveness of VIF, we provide an intuitive analysis from an information theoretic perspective.

In standard MLLMs, the next token generation probability can be expressed as $p(o_l | o_{<l}, Z^t, Z^v)$, where the visual condition Z^v remains static throughout decoding. As generation proceeds, the textual context $o_{<l}$ grows while Z^v stays unchanged. Consequently, the model gradually relies more on textual history, and the mutual information between the output token and the visual modality,

$$I(o_l; Z^v | Z^t, o_{<l}), \quad (10)$$

tends to diminish. This reflects visual consistency decay as the generation extends. Our proposed VIF addresses this issue by introducing a dynamic visual inference variable, $A_l = f(Z^v, h_l)$, which adaptively refines the visual representation conditioned on the evolving hidden state. This mechanism transforms the generation process into $p(o_l |$

$o_{<l}, Z^t, Z^v, A_l)$, where A_l acts as a context-dependent bridge between visual and linguistic spaces. From the viewpoint of mutual information, this modification expands the dependency set to include a context-aware variable.

$$I(o_l; Z^v, A_l | Z^t, o_{<l}). \quad (11)$$

Since A_l is derived from both Z^v and the current linguistic state h_l , it introduces an additional pathway through which visual information can influence the token generation. By the monotonicity of mutual information [7],

$$\begin{aligned} I(o_l; Z^v, A_l | Z^t, o_{<l}) &= I(o_l; Z^v | Z^t, o_{<l}) \\ &\quad + I(o_l; A_l | Z^v, Z^t, o_{<l}) \\ &\geq I(o_l; Z^v | Z^t, o_{<l}). \end{aligned} \quad (12)$$

Hence, the dynamic conditioning established by VIF increases the mutual information between output tokens and visual signals, explaining its ability to maintain visual consistency across the entire decoding process.

5. Experiments

5.1. Experimental setup

Evaluation benchmarks. We conducted extensive evaluations across a comprehensive set of 14 benchmark datasets, including MMMU [45], RealWorldQA [43], MMBench [22], MMStar [4], OK-VQA [24], GQA [13], ScienceQA [32], MMVP [39], OCRBench [21], TextVQA [34], AI2D [12], InfographicVQA [27], DocVQA [26] and POPE [19]. These benchmarks span multiple domains such as general

Table 2. Performance comparison on text related benchmarks.

Method	Params	OCRBench	TextVQA	AI2D	DocVQA	InfographicVQA	Average
GPT-4V-1106	-	645	78.0	78.2	88.4	-	-
Gemini Pro	-	680	74.6	-	88.1	-	-
Cambrian-1	8B	624	71.7	73.0	77.8	-	-
mPLUG-Owl3	8B	-	69.0	73.4	-	-	-
Ross	7B	-	-	69.30	-	-	-
<i>Base model: Qwen-2.5-VL</i>							
Qwen2.5-VL	7B	732	74.56	82.38	95.70	81.47	81.46
Qwen2.5-VL-SFT	7B	724	74.02	83.67	94.80	81.36	81.25
Qwen2.5-VL-VIF	7B	747	74.86	85.78	<u>95.50</u>	83.14	82.80
<i>Base model: LLaVA-1.5</i>							
VISTA	7B	321	46.63	56.28	22.66	-	-
LLaVA-1.5	7B	275	38.87	55.44	31.45	28.17	36.29
LLaVA-1.5-SFT	7B	336	40.30	62.95	39.77	28.58	41.04
LLaVA-1.5-VIF	7B	346	<u>46.28</u>	64.90	44.79	29.95	44.10
LLaVA-1.5	13B	301	41.54	58.94	34.39	30.35	39.06
LLaVA-1.5-SFT	13B	347	47.52	66.41	41.89	31.73	44.45
LLaVA-1.5-VIF	13B	352	48.04	68.62	46.68	32.71	46.25

multimodal understanding, knowledge reasoning, hallucination detection, optical character recognition and chart comprehension, enabling a thorough assessment of the model’s VQA capabilities across diverse scenarios.

Models. We evaluate the proposed method across both fixed-resolution and dynamic-resolution model backbones to comprehensively assess its generality. In particular, LLaVA-1.5 [20] serves as the representative fixed-resolution model, while Qwen2.5-VL [2] is adopted as the dynamic-resolution counterpart. For LLaVA-1.5, we conduct experiments on both the 7B and 13B variants, adhering to the official configuration that utilizes CLIP-ViT-L/14-336 [30] as the vision encoder. For Qwen2.5-VL, all evaluations are performed using the 7B parameter scale.

Baselines. To comprehensively evaluate the effectiveness of our method, we compare it not only with the base models and a standard supervised fine-tuning (SFT) baseline trained on the exact same data to isolate the algorithmic improvements, but also with a broad range of competitive multimodal large language models. Specifically, we include proprietary systems such as GPT-4V-1106 [29] and Gemini Pro [36], as well as recent state-of-the-art open-source models of comparable scale, including Cambrian-1 [37], Ross[40], mPLUG-Owl3 [44], and VISTA [18]. This comprehensive selection ensures that our evaluation spans diverse architectures, training paradigms, and data settings, enabling a fair and representative comparison across both closed-source and open-source ecosystems.

Training. Our training pipeline is organized into three sequential stages to ensure stable optimization and effective convergence. (1) *Warm-up stage*: only the proposed

inference former and the LLM head are trained on a small-scale pre-training dataset, while all other parameters are kept frozen. This stage serves to initialize the newly introduced components and stabilize early training. (2) *Pretraining stage*: we then perform full model fine-tuning on the complete training corpus to enable global adaptation across both visual and textual modalities. (3) *Instruction tuning stage*: following the protocol in Ross [40], we further refine the model using a subset of the Cambrian [37] dataset to enhance instruction following capability while preventing potential data leakage. Each stage is trained for one epoch. All experiments are conducted on a server with eight NVIDIA H200 GPUs (140GB each), using DeepSpeed [31] to support efficient distributed optimization. We adopt a cosine learning rate decay schedule with a 3% warm-up ratio, and set the maximum sequence length to 4096 tokens. Additional training details are provided in Appendix 7.2.

5.2. Main results

In this section, we present a comprehensive analysis of experimental results. As shown in Table 1 2 3, VIF consistently enhances multimodal ability across various tasks. Overall, our method achieves state-of-the-art performance, demonstrating its robustness and effectiveness across diverse model architectures and evaluation benchmarks.

Results on general and knowledge VQA benchmarks.

As presented in Table 1, our method exhibits consistently strong performance across a variety of general and knowledge VQA benchmarks. For the Qwen2.5-VL 7B model, integrating the proposed VIF module yields consistent improvements across six datasets, increasing the average score

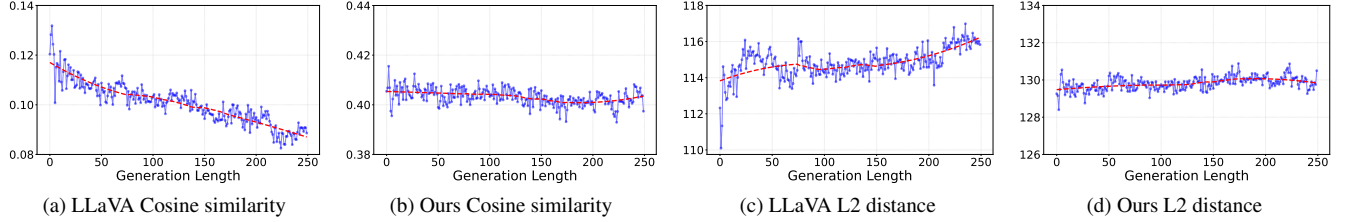


Figure 4. Evolution of image–text correlation during generation. We evaluate the evolution of image–text correlation during generation on the RealWorldQA dataset, comparing LLaVA-1.5-7B and our method. Specifically, we compute the average cosine similarity and L2 distance between each generated token and all decoded image tokens, and report their mean values over the entire dataset. The red curve represents the smoothed trend obtained using a Savitzky–Golay filter.

from 70.92 to 73.08, resulting in an absolute gain of 2.16 percentage points, highlighting the overall effectiveness of VIF in improving multimodal understanding. For LLaVA-1.5-based models, our method achieves state-of-the-art performance across all benchmarks. Specifically, the 7B variant attains an average improvement of 1.64 percentage points across six datasets, outperforming baselines by a substantial margin. Furthermore, the LLaVA-1.5-13B variant equipped with our VIF module also establishes new state-of-the-art results across all benchmarks, achieving an average improvement of 1.11 percentage points. These consistent improvements across multiple datasets and model scales demonstrate that the proposed VIF module effectively enhances the model’s ability to attend to and reason over visual content. By reinforcing the alignment between visual evidence and textual understanding, our approach enables more accurate and robust multimodal reasoning.

Results on text related benchmarks. We report the performance of VIF on text-related benchmarks in Table 2, including OCR datasets and chart understanding datasets. Our method consistently enhances the models’ abilities in recognizing textual content and interpreting structured visual information. For the Qwen2.5-VL model, VIF yields an average improvement of 1.55 percentage points on all five datasets. Even more significant improvements are observed with LLaVA-1.5 models. The 7B version achieves an average gain of 3.06 percentage points. Similarly, the 13B version attains an average enhancement of 1.80 percentage points. Overall, VIF achieves state-of-the-art results across most benchmarks, demonstrating its effectiveness in enhancing text understanding and structured reasoning in multimodal tasks.

Results on vision centric and hallucination benchmarks. To further validate the capability of the proposed VIF module, we extend our evaluation to vision-centric and hallucination benchmarks in Table 3, including RealWorldQA, MMVP, and POPE. The experimental results demonstrate that our method achieves significant performance improvements across all these challenging tasks. As detailed in our evaluation, VIF brings consistent enhancements to various model architectures. For the Qwen2.5-VL

7B model, we observe improvements of 2.09, 3.00, and 1.02 percentage points on RealWorldQA, MMVP, and POPE, respectively. The LLaVA-1.5-7B model shows even more pronounced gains, achieving performance boosts of 2.22, 6.00, and 0.94 percentage points across the three benchmarks. Similarly, the LLaVA-1.5-13B model exhibits enhancements of 1.70, 1.67, and 2.81 percentage points on the respective datasets. These consistent improvements across diverse vision-centric and hallucination benchmarks provide compelling additional evidence for the effectiveness of the VIF module in enhancing multimodal reasoning capabilities. The results highlight VIF’s strength in improving visual capability and reducing model hallucinations, which are critical challenges in vision language applications.

Table 3. Performance comparison on vision centric and hallucination benchmarks. RWQA stands for RealWorldQA dataset.

Method	Params	RWQA	MMVP	POPE
GPT-4V-1106	-	63.0	50.0	75.4
Gemini Pro	-	60.4	-	-
Cambrian-1	8B	64.2	51.3	87.4
mPLUG-Owl3	8B	60.4	-	88.2
Ross	7B	-	39.3	88.2
<i>Base model: Qwen-2.5-VL</i>				
Qwen2.5-VL	7B	68.63	70.33	88.03
Qwen2.5-VL-SFT	7B	68.37	73.00	87.69
Qwen2.5-VL-VIF	7B	70.46	76.00	88.71
<i>Base model: LLaVA-1.5</i>				
VISTA	7B	56.34	-	-
LLaVA-1.5	7B	55.95	24.70	86.90
LLaVA-1.5-SFT	7B	55.56	47.33	86.93
LLaVA-1.5-VIF	7B	57.78	53.33	87.87
LLaVA-1.5	13B	54.90	63.33	85.32
LLaVA-1.5-SFT	13B	55.29	65.00	85.52
LLaVA-1.5-VIF	13B	56.99	66.67	88.33

5.3. Visualization results

To further investigate how our method enhances visual capability during text generation, we analyze the evolution

of vision-language alignment on the RealWorldQA dataset. Specifically, we compute the average cosine similarity and L2 distance between each generated text token and the decoded visual token sequence, and report the mean values over all samples. The results are visualized in Figure 4.

Analysis of cosine similarity. As shown in Figure 4a, the original LLaVA model exhibits a noticeable degradation in image alignment as the generation length increases, with cosine similarity gradually decreasing over the generation process. This pattern indicates that the baseline model gradually drifts away from visual semantics and relies increasingly on linguistic priors. In contrast, our method maintains a relatively stable cosine similarity, as reflected in Figure 4b, suggesting that the VIF module effectively preserves the visual grounding signal within the decoder.

Analysis of L2 distance. Similarly, the L2 distance analysis in Figure 4c reveals that the original model shows an increasing divergence from visual features as generation progresses, with L2 distance steadily rising. This trend further confirms the baseline model’s tendency to deviate from image-conditioned semantics during extended generation. Our approach consistently maintains a relatively stable L2 distance throughout the generation sequence (Figure 4d), indicating that the VIF module successfully prevents the loss of visual alignment during autoregressive generation.

Overall, these results demonstrate that our approach not only improves task performance on benchmark evaluations but also strengthens the model’s internal consistency between generated text and visual content, thereby offering a more interpretable and robust visual reasoning process.

5.4. Ablation study

In this section, we present ablation studies covering computational efficiency and architectural analysis.

Computational efficiency analysis. We evaluate the efficiency of our method on five datasets by measuring inference latency and GPU memory consumption relative to the LLaVA-1.5-7B baseline. All experiments are conducted on a single GPU without batch processing to ensure accurate resource measurement. As shown in Table 4, LLaVA-1.5-VIF introduces only minor overhead, with an average inference time of $1.04\times$ and GPU memory usage of $1.05\times$ compared to the baseline. These results demonstrate that our method preserves the high efficiency and scalability of the original model with negligible additional cost.

Ablation study on architecture. To assess the contribution of the self-attention layer in VIF, we perform an ablation experiment. As shown in Table 5, introducing a self-attention layer consistently improves performance across most settings. This highlights the crucial role of the self-attention layer in capturing key feature dependencies.

Table 4. Inference time and GPU memory usage comparison across different benchmarks. MMS stands for MMStar, RW stands for RealWorldQA, TQA stands for TextVQA, and MMB stands for MMBench. All experiments are conducted on a single GPU without batch processing.

Method	MMS	RW	AI2D	MMB	TQA	Avg
<i>Time cost (measured in seconds)</i>						
LLaVA	90.2	79.9	197.1	251.5	436.4	x1.0
LLaVA-VIF	94.4	81.2	201.5	262.5	465.5	x1.04
<i>GPU memory cost (measured in GB)</i>						
LLaVA	15.7	15.1	15.2	15.1	14.9	x1.0
LLaVA-VIF	16.5	15.8	16.1	16.6	15.6	x1.05

Table 5. The impact of removing self-attention layers in VIF on model performance.

Method	RWQA	MMStar	AI2D	MMVP
LLaVA-7B	55.95	33.00	55.44	24.70
LLaVA-VIF-7B	57.78	37.56	64.90	53.33
wo/self-attn layer	56.21	36.07	64.50	49.67
LLaVA-13B	54.90	33.87	58.94	63.33
LLaVA-VIF-13B	56.99	41.07	68.62	66.67
wo/self-attn layer	56.00	41.87	67.94	66.67

6. Conclusion

In this paper, we address the challenge of visual consistency decay in multimodal large language models. Our study emphasizes the necessity of dynamic and sustained vision-language interaction, rather than treating visual inputs as static, one-time context. To this end, we proposed the Visual Inference Former, a simple yet effective architecture that dynamically reinforces visual grounding throughout the autoregressive decoding process. By enabling fine-grained and continuous interaction between evolving textual representations and visual features, VIF ensures that visual information remains an active and influential component during generation, thereby alleviating the degradation of visual grounding. Extensive experiments across multiple architectures and evaluation benchmarks demonstrate that VIF consistently improves visual consistency and reasoning performance with minimal computational overhead.

Despite its effectiveness, VIF still has limitations. Our current design focuses on static image reasoning, and the direct integration of full visual representations may face scalability issues in high-cost scenarios such as video understanding. Moreover, the simple additive fusion strategy, though efficient, may not fully capture complex cross-modal dependencies. Future work will explore more adaptive and expressive fusion mechanisms to further enhance multimodal reasoning capabilities.

Acknowledgements

This work was supported in part by the Key Research and Development Program of Zhejiang Province (2026C01021), "Pioneer" and "Leading Goose" R&D Program of Zhejiang (2025C02037), and National Natural Science Foundation of China (No. 62376243). All opinions in this paper are those of the authors and do not necessarily reflect the views of the funding agencies.

References

- [1] Peter Anderson, Xiaodong He, Chris Buehler, Damien Teney, Mark Johnson, Stephen Gould, and Lei Zhang. Bottom-up and top-down attention for image captioning and visual question answering. In *Proceedings of the IEEE conference on computer vision and pattern recognition*, pages 6077–6086, 2018. 3
- [2] Shuai Bai, Keqin Chen, Xuejing Liu, Jialin Wang, Wenbin Ge, Sibao Song, Kai Dang, Peng Wang, Shijie Wang, Jun Tang, et al. Qwen2. 5-vl technical report. *arXiv preprint arXiv:2502.13923*, 2025. 6
- [3] Lin Chen, Jinsong Li, Xiaoyi Dong, Pan Zhang, Conghui He, Jiaqi Wang, Feng Zhao, and Dahua Lin. Sharegpt4v: Improving large multi-modal models with better captions. In *European Conference on Computer Vision*, pages 370–387. Springer, 2024. 1
- [4] Lin Chen, Jinsong Li, Xiaoyi Dong, Pan Zhang, Yuhang Zang, Zehui Chen, Haodong Duan, Jiaqi Wang, Yu Qiao, Dahua Lin, et al. Are we on the right way for evaluating large vision-language models? *arXiv preprint arXiv:2403.20330*, 2024. 5, 1
- [5] Zhe Chen, Jiannan Wu, Wenhai Wang, Weijie Su, Guo Chen, Sen Xing, Muyan Zhong, Qinglong Zhang, Xizhou Zhu, Lewei Lu, et al. Internvl: Scaling up vision foundation models and aligning for generic visual-linguistic tasks. In *Proceedings of the IEEE/CVF conference on computer vision and pattern recognition*, pages 24185–24198, 2024. 3
- [6] Xu Chu, Xinrong Chen, Guanyu Wang, Zhijie Tan, Kui Huang, Wenyu Lv, Tong Mo, and Weiping Li. Qwen look again: Guiding vision-language reasoning models to re-attention visual information. *arXiv preprint arXiv:2505.23558*, 2025. 1, 3
- [7] Thomas M Cover. *Elements of information theory*. John Wiley & Sons, 1999. 5
- [8] Wenliang Dai, Junnan Li, Dongxu Li, Anthony Tiong, Junqi Zhao, Weisheng Wang, Boyang Li, Pascale N Fung, and Steven Hoi. Instructblip: Towards general-purpose vision-language models with instruction tuning. *Advances in neural information processing systems*, 36:49250–49267, 2023. 3
- [9] Alexey Dosovitskiy. An image is worth 16x16 words: Transformers for image recognition at scale. *arXiv preprint arXiv:2010.11929*, 2020. 3
- [10] Enrico Fini, Mustafa Shukor, Xiujun Li, Philipp Dufter, Michal Klein, David Haldimann, Sai Aitharaju, Victor G Turrisi da Costa, Louis Béthune, Zhe Gan, et al. Multi-modal autoregressive pre-training of large vision encoders. In *Proceedings of the Computer Vision and Pattern Recognition Conference*, pages 9641–9654, 2025. 3
- [11] Yash Goyal, Tejas Khot, Douglas Summers-Stay, Dhruv Batra, and Devi Parikh. Making the v in vqa matter: Elevating the role of image understanding in visual question answering. In *Proceedings of the IEEE conference on computer vision and pattern recognition*, pages 6904–6913, 2017. 1
- [12] Tuomo Hiippala, Malihe Alikhani, Jonas Haverinen, Timo Kalliokoski, Evanfiya Logacheva, Serafina Orekhova, Aino Tuomainen, Matthew Stone, and John A Bateman. Ai2d-rst: a multimodal corpus of 1000 primary school science diagrams. *Language Resources and Evaluation*, 55(3):661–688, 2021. 5, 1
- [13] Drew A Hudson and Christopher D Manning. Gqa: A new dataset for real-world visual reasoning and compositional question answering. In *Proceedings of the IEEE/CVF conference on computer vision and pattern recognition*, pages 6700–6709, 2019. 5, 1
- [14] Chao Jia, Yinfei Yang, Ye Xia, Yi-Ting Chen, Zarana Parekh, Hieu Pham, Quoc Le, Yun-Hsuan Sung, Zhen Li, and Tom Duerig. Scaling up visual and vision-language representation learning with noisy text supervision. In *International conference on machine learning, ICML*, pages 4904–4916, 2021. 3
- [15] Kushal Kafle, Scott Cohen, Brian Price, and Christopher Kanan. Dvqa: Understanding data visualizations via question answering. In *CVPR*, 2018. 1
- [16] Sicong Leng, Hang Zhang, Guanzheng Chen, Xin Li, Shijian Lu, Chunyan Miao, and Lidong Bing. Mitigating object hallucinations in large vision-language models through visual contrastive decoding. In *Proceedings of the IEEE/CVF Conference on Computer Vision and Pattern Recognition*, pages 13872–13882, 2024. 1
- [17] Junnan Li, Dongxu Li, Silvio Savarese, and Steven Hoi. Blip-2: Bootstrapping language-image pre-training with frozen image encoders and large language models. In *International conference on machine learning*, pages 19730–19742. PMLR, 2023. 3
- [18] Mingxiao Li, Na Su, Fang Qu, Zhizhou Zhong, Ziyang Chen, Yuan Li, Zhaopeng Tu, and Xiaolong Li. Vista: Enhancing vision-text alignment in mllms via cross-modal mutual information maximization. *arXiv preprint arXiv:2505.10917*, 2025. 3, 6
- [19] Yifan Li, Yifan Du, Kun Zhou, Jinpeng Wang, Wayne Xin Zhao, and Ji-Rong Wen. Evaluating object hallucination in large vision-language models. *arXiv preprint arXiv:2305.10355*, 2023. 5, 1
- [20] Haotian Liu, Chunyuan Li, Qingyang Wu, and Yong Jae Lee. Visual instruction tuning. *Advances in neural information processing systems*, 36, 2024. 1, 3, 6
- [21] Yuliang Liu, Zhang Li, Mingxin Huang, Biao Yang, Wenwen Yu, Chunyuan Li, Xu-Cheng Yin, Cheng-Lin Liu, Lianwen Jin, and Xiang Bai. Ocrbench: on the hidden mystery of ocr in large multimodal models. *Science China Information Sciences*, 67(12):220102, 2024. 5, 1
- [22] Yuan Liu, Haodong Duan, Yuanhan Zhang, Bo Li, Songyang Zhang, Wangbo Zhao, Yike Yuan, Jiaqi Wang, Conghui He,

- Ziwei Liu, et al. Mmbench: Is your multi-modal model an all-around player? In *European conference on computer vision*, pages 216–233. Springer, 2025. 5, 1
- [23] Jiasen Lu, Dhruv Batra, Devi Parikh, and Stefan Lee. Vilbert: Pretraining task-agnostic visiolinguistic representations for vision-and-language tasks. *Advances in neural information processing systems*, 32, 2019. 3
- [24] Kenneth Marino, Mohammad Rastegari, Ali Farhadi, and Roozbeh Mottaghi. Ok-vqa: A visual question answering benchmark requiring external knowledge. In *Proceedings of the IEEE/cvf conference on computer vision and pattern recognition*, pages 3195–3204, 2019. 5, 1
- [25] Ahmed Masry, Do Long, Jia Qing Tan, Shafiq Joty, and Enamul Hoque. ChartQA: A benchmark for question answering about charts with visual and logical reasoning. In *Findings of the Association for Computational Linguistics: ACL 2022*, pages 2263–2279, Dublin, Ireland, 2022. Association for Computational Linguistics. 1
- [26] Minesh Mathew, Dimosthenis Karatzas, and CV Jawahar. Docvqa: A dataset for vqa on document images. In *Proceedings of the IEEE/CVF winter conference on applications of computer vision*, pages 2200–2209, 2021. 5, 1
- [27] Minesh Mathew, Viraj Bagal, Rubèn Tito, Dimosthenis Karatzas, Ernest Valveny, and CV Jawahar. Infographicvqa. In *Proceedings of the IEEE/CVF Winter Conference on Applications of Computer Vision*, pages 1697–1706, 2022. 5, 1
- [28] Anand Mishra, Shashank Shekhar, Ajeet Kumar Singh, and Anirban Chakraborty. Ocr-vqa: Visual question answering by reading text in images. In *2019 international conference on document analysis and recognition (ICDAR)*, pages 947–952. IEEE, 2019. 1
- [29] OpenAI. GPT-4V(ision) System Card, 2023. 1, 6
- [30] Alec Radford, Jong Wook Kim, Chris Hallacy, Aditya Ramesh, Gabriel Goh, Sandhini Agarwal, Girish Sastry, Amanda Askell, Pamela Mishkin, Jack Clark, et al. Learning transferable visual models from natural language supervision. pages 8748–8763, 2021. 3, 6
- [31] Jeff Rasley, Samyam Rajbhandari, Olatunji Ruwase, and Yuxiong He. Deepspeed: System optimizations enable training deep learning models with over 100 billion parameters. In *Proceedings of the 26th ACM SIGKDD international conference on knowledge discovery & data mining*, pages 3505–3506, 2020. 6
- [32] Tanik Saikh, Tirthankar Ghosal, Amish Mittal, Asif Ekbal, and Pushpak Bhattacharyya. Scienceqa: A novel resource for question answering on scholarly articles. *International Journal on Digital Libraries*, 23(3):289–301, 2022. 5, 1
- [33] Ronald W Schafer. What is a savitzky-golay filter?[lecture notes]. *IEEE Signal processing magazine*, 28(4):111–117, 2011. 2
- [34] Amanpreet Singh, Vivek Natarajan, Meet Shah, Yu Jiang, Xinlei Chen, Dhruv Batra, Devi Parikh, and Marcus Rohrbach. Towards vqa models that can read. In *Proceedings of the IEEE/CVF conference on computer vision and pattern recognition*, pages 8317–8326, 2019. 5, 1
- [35] Wei Suo, Lijun Zhang, Mengyang Sun, Lin Yuanbo Wu, Peng Wang, and Yanning Zhang. Octopus: Alleviating hallucination via dynamic contrastive decoding. In *Proceedings of the Computer Vision and Pattern Recognition Conference*, pages 29904–29914, 2025. 1
- [36] Gemini Team, Rohan Anil, Sebastian Borgeaud, Jean-Baptiste Alayrac, Jiahui Yu, Radu Soricut, Johan Schalkwyk, Andrew M Dai, Anja Hauth, Katie Millican, et al. Gemini: a family of highly capable multimodal models. *arXiv preprint arXiv:2312.11805*, 2023. 1, 6
- [37] Shengbang Tong, Ellis Brown, Penghao Wu, Sanghyun Woo, Manoj Middepogu, Sai Charitha Akula, Jihan Yang, Shusheng Yang, Adithya Iyer, Xichen Pan, et al. Cambrian-1: A fully open, vision-centric exploration of multimodal llms. *arXiv preprint arXiv:2406.16860*, 2024. 6, 1
- [38] Shengbang Tong, David Fan, Jiachen Zhu, Yunyang Xiong, Xinlei Chen, Koustuv Sinha, Michael Rabbat, Yann LeCun, Saining Xie, and Zhuang Liu. Metamorph: Multimodal understanding and generation via instruction tuning. *arXiv preprint arXiv:2412.14164*, 2024. 3
- [39] Shengbang Tong, Zhuang Liu, Yuexiang Zhai, Yi Ma, Yann LeCun, and Saining Xie. Eyes wide shut? exploring the visual shortcomings of multimodal llms. In *Proceedings of the IEEE/CVF Conference on Computer Vision and Pattern Recognition*, pages 9568–9578, 2024. 5, 1
- [40] Haochen Wang, Anlin Zheng, Yucheng Zhao, Tiancai Wang, Zheng Ge, Xiangyu Zhang, and Zhaoxiang Zhang. Reconstructive visual instruction tuning. *arXiv preprint arXiv:2410.09575*, 2024. 3, 6, 1
- [41] Ke Wang, Junting Pan, Weikang Shi, Zimu Lu, Houxing Ren, Aojun Zhou, Mingjie Zhan, and Hongsheng Li. Measuring multimodal mathematical reasoning with math-vision dataset. *Advances in Neural Information Processing Systems*, 37:95095–95169, 2024. 1
- [42] Peng Wang, Shuai Bai, Sinan Tan, Shijie Wang, Zhihao Fan, Jinze Bai, Keqin Chen, Xuejing Liu, Jialin Wang, Wenbin Ge, et al. Qwen2-vl: Enhancing vision-language model’s perception of the world at any resolution. *arXiv preprint arXiv:2409.12191*, 2024. 3
- [43] x.ai. Grok-1.5 vision preview, 2024. Accessed: 2025-01-26. 5, 1
- [44] Jiabo Ye, Haiyang Xu, Haowei Liu, Anwen Hu, Ming Yan, Qi Qian, Ji Zhang, Fei Huang, and Jingren Zhou. mplug-owl3: Towards long image-sequence understanding in multi-modal large language models. *arXiv preprint arXiv:2408.04840*, 2024. 3, 6
- [45] Xiang Yue, Yuansheng Ni, Kai Zhang, Tianyu Zheng, Ruoqi Liu, Ge Zhang, Samuel Stevens, Dongfu Jiang, Weiming Ren, Yuxuan Sun, et al. Mmmu: A massive multi-discipline multimodal understanding and reasoning benchmark for expert agi. In *Proceedings of the IEEE/CVF Conference on Computer Vision and Pattern Recognition*, pages 9556–9567, 2024. 5, 1
- [46] Li Yujian and Liu Bo. A normalized levenshtein distance metric. *IEEE transactions on pattern analysis and machine intelligence*, 29(6):1091–1095, 2007. 1
- [47] Yi-Fan Zhang, Weichen Yu, Qingsong Wen, Xue Wang, Zhang Zhang, Liang Wang, Rong Jin, and Tieniu Tan. De-

biasing multimodal large language models. *arXiv preprint arXiv:2403.05262*, 2024. 1

- [48] Deyao Zhu, Jun Chen, Xiaoqian Shen, Xiang Li, and Mohamed Elhoseiny. Minigpt-4: Enhancing vision-language understanding with advanced large language models. *arXiv preprint arXiv:2304.10592*, 2023. 3
- [49] Jinguo Zhu, Weiyun Wang, Zhe Chen, Zhaoyang Liu, Shenglong Ye, Lixin Gu, Hao Tian, Yuchen Duan, Weijie Su, Jie Shao, et al. Internvl3: Exploring advanced training and test-time recipes for open-source multimodal models. *arXiv preprint arXiv:2504.10479*, 2025. 3

Vision Inference Former: Sustaining Visual Consistency in Multimodal Large Language Models

Supplementary Material

7. Experimental details

In this section, we present the specific experimental setting including benchmarks and train details.

7.1. Benchmarks

We conducted extensive evaluations across a comprehensive set of 14 benchmark datasets, including MMMU [45], RealWorldQA [43], MMBench [22], MMStar [4], OK-VQA [24], GQA [13], ScienceQA [32], and MMVP [39], OCRBench [21], TextVQA [34], AI2D [12], InfographicVQA [27], DocVQA [26] and POPE [19].

For DocVQA and InfographicVQA, we adopt the Average Normalized Levenshtein Similarity (ANLS) metric [46], while for all other datasets, we report standard accuracy metrics.

7.2. Train details

All experiments are conducted on a high-performance server equipped with eight NVIDIA H200 GPUs, each with 140 GB of memory. We employ DeepSpeed to enable efficient distributed training and memory optimization. The learning rate follows a cosine decay schedule with a 3% warm-up ratio, ensuring stable convergence during the early training phase. The maximum sequence length is set to 4096 tokens to accommodate long-context multimodal interactions.

Detailed hyperparameter configurations for training LLaVA and Qwen2.5-VL are provided in Table 6 and Table 7, respectively.

Our training pipeline consists of three sequential stages designed to ensure stable optimization and effective convergence: (1) Warm-up stage. We first train only the proposed Vision Inference Former and the LLM head on a small-scale pretraining dataset, while freezing all other parameters. This stage serves to initialize the newly introduced components and stabilize the optimization dynamics in the early phase. (2) Pretraining stage. Next, we conduct full-model fine-tuning on the complete multimodal corpus, enabling the model to achieve global adaptation across both visual and textual modalities. (3) Instruction tuning stage. Following the protocol of Ross [40], we further refine the model using a subset of the Cambrian dataset [37] to strengthen instruction-following capability while mitigating the risk of data leakage.

The pretraining corpus comprises LLaVA-Pretrain [20] and ShareGPT4V [3], which provide broad visual-language coverage for model initialization.

Table 6. Hyperparameters of training LLaVA.

Config	Step1	Step2	Step3
Trainable parts	VIF+LLM head	ALL	ALL
Global batch size	128	128	256
Batch size per GPU	8	8	16
Global learning rate	1e-4	2e-5	2e-5
Former learning rate	1e-4	4e-5	4e-5
Accumulated steps		2	
DeepSpeed zero stage		3	
Learning rate schedule	warmup + cosine decay		
Warmup ratio		0.03	
Weight decay		0	
Epoch		1	
Optimizer		AdamW	
Precision		bfloat16	
Model max length		4096	

Table 7. Hyperparameters of training Qwen2.5-VL.

Config	Step1	Step2	Step3
Trainable parts	VIF+LLM head	ALL	ALL
Global batch size	128	128	256
Batch size per GPU	8	8	16
Global learning rate	1e-4	1e-5	1e-5
Former learning rate	1e-4	2e-5	2e-5
Accumulated steps		2	
DeepSpeed zero stage		3	
Learning rate schedule	warmup + cosine decay		
Warmup ratio		0.03	
Weight decay		0	
Epoch		1	
Optimizer		AdamW	
Precision		bfloat16	
Model max length		4096	

The instruction tuning dataset includes LLaVA-Instruct, VQAv2 [11], GQA [13], OCRVQA [28], TextVQA [34], DVQA [15], DocVQA [26], ChartQA [25], ScienceQA [32], and MathVision [41].

For GQA, OCRVQA, TextVQA, DocVQA, and ScienceQA, we use the training splits for instruction tuning.

Table 8. Details of the instruction tuning dataset.

Method	Samples
LLaVA-Instruct	665k
VQAv2	240k
GQA_train	700k
OCRVQA_train	80k
TextVQA_train	34k
DVQA	39k
DocVQA_train	20k
ChartQA	2.5k
SciencQA_train	6k
MathVision	3k

Table 9. Details of the pre-train dataset.


Method	Samples
LLaVA-Pretrain	558k
ShareGPT4V	80k

8. Case study

To qualitatively assess how the proposed Vision Inference Former (VIF) enhances visual grounding and reasoning consistency, we present representative case studies comparing LLaVA-1.5-7B and our LLaVA-VIF on visual question answering and image description tasks.

As shown in Figure 5, the question asks: “Where is the woman’s blue bag located in the image?” The baseline LLaVA-1.5-7B predicts “In her hand,” whereas LLaVA-VIF correctly answers “On her shoulder.” This case exemplifies a common failure of connector-based models—the model’s attention gradually shifts toward linguistic priors (e.g., the frequent co-occurrence of “hand” and “bag”) instead of true visual evidence. By continuously injecting visual semantics into the decoding hidden states, VIF maintains stable alignment between the generated representation and the underlying visual features, resulting in an accurate and visually grounded answer.


In a free-form image description task (Figure 6), the baseline LLaVA-1.5-7B correctly described the image content in the early stages, but deviated in the latter half. In contrast, LLaVA-VIF identifies these details and provides a coherent, context-aware narrative of the scene. This improvement demonstrates VIF’s ability to reinforce high-level semantic integration by directly linking decoding hidden states to uncompressed visual representations, thus preventing the loss of contextual cues during generation.



User:
Where is the woman's blue bag located in the image?
Options:
A: In her hand
B: On her shoulder
C: On the ground
D: Inside the man's bag

LLaVA: A
LLaVA-VIF: B

Figure 5. Case study in MMStar.



User: Describe this image.

LLaVA : The image features a sidewalk with a row of orange and white traffic cones placed along it. The cones are positioned in a straight line, creating a barrier to direct pedestrian traffic. There are a total of nine cones in the scene, with some closer to the foreground and others further back. In the background, there are two cars parked on the street, **one on the left side and the other on the right side of the image. Additionally, there is a person standing near the middle of the scene, possibly observing the traffic cones or walking by.**

LLaVA-VIF: The image captures a scene of a construction site or road work area. The main focus is a row of orange and white traffic cones, which are lined up along a sidewalk. These cones are connected by yellow caution tape, creating a barrier to guide pedestrians and vehicles safely around the work zone. The background of the image reveals a house and a tree, providing a sense of the location and context of the construction site. The overall scene suggests ongoing work or maintenance in the area, with the cones and tape serving as a visual indication of the ongoing activity.

Figure 6. Case study.